Majorana fermions in semiconductor nanostructures with two wires connected through a ring

B Y Sun and M W Wu

Hefei National Laboratory for Physical Sciences at Microscale and Department of Physics, University of Science and Technology of China, Hefei, Anhui 230026, People's Republic of China

E-mail: mwwu@ustc.edu.cn

Abstract

We investigate the Majorana fermions in a semiconductor nanostructure with two wires connected through a ring. The nanostructure is mirror symmetric and in the proximity of a superconductor. The Rashba spin–orbit coupling and a magnetic field parallel to the wires or perpendicular to the ring are included. Moreover, a magnetic flux is applied through the center of the ring, which makes the phase difference of the superconducting order parameters in the two wires being zero or π due to the fluxoid quantization and the thermodynamic equilibrium of the supercurrent in the superconducting ring. If the phase difference is π, two Majorana modes are shown to appear around the ring without interacting with each other. In contrast, if the phase difference is zero, these Majorana modes disappear and the states localized around the ring have finite energies. These states can be detected via the conductance measurement by connecting two normal leads to the wires and a third one directly to the ring. It is shown in the bias dependence of the differential conductance from one of the leads connected to the wire to the one connected directly to the ring that the tunnelings through the Majorana modes (i.e., in the case with π phase difference) leads to two peaks very close to the zero bias, while the tunneling through the states with finite energies (i.e., in the case with zero phase difference) leads to peaks far away from the zero bias if the ring radius is small. This difference for the cases

with and without the Majorana modes in small ring radius is distinct and hence can be used to identify the Majorana modes.

1. Introduction

In recent years, Majorana fermions have attracted immense attention due to their possible applications in quantum computation [1–7]. They are proposed to exist in various systems [3, 8–21] and many experimental attempts have been devoted to identify them [22–29]. Among these attempts, the zero-bias conductance peak [30–36] is a characteristic property from the Majorana modes which is often detected. This conductance measurement is easy to perform and the zero-bias conductance peak has already been observed [24–29]. Nevertheless, these experimental results can not serve as decisive evidence since the zero-bias conductance peak can appear due to many other mechanisms [37–40]. Hence, to further identify the Majorana fermions, the comprehension and detection of more transport properties at different Majorana configurations are needed.

Among the works investigating Majorana nanostructures, the system of two connected nanostructures with different order parameter phases is often investigated. It is found in various materials [41–44] that when this phase difference is π, two Majorana modes can appear around the contacting point. Although they are close, these Majorana modes do not interact with each other, which is quit different from the result that the Majorana fermions at the adjacent ends of the nanowire interact with each other due to their wave-function overlapping [45]. Inspired by these results, we propose a semiconductor nanostructure with two wires connected through a ring as illustrated in figure 1. The nanostructure is in the proximity of a superconductor. With a magnetic flux ϕ through the superconducting ring, the variation of the supercurrent in the superconductor ring is governed by the fluxoid quantization and the thermodynamic equilibrium [46]. Then, due to the proximity effect, the order parameter in the semiconductor ring varies as [46]

$$\Delta(\theta) = |\Delta_0| \, \exp\left(i\left[2\phi/\phi_0\right]\theta\right). \tag{1}$$

Here, $[x]$ denotes the integer closest to x (if x is a half-integer, it is rounded up) and $\phi_0 = h/e$ is the flux quantum. Since the phase difference of the order parameters between the left ($\theta = 0$) and right ($\theta = \pi$) wires is $[2\phi/\phi_0]\pi$, Majorana fermions are expected to appear around the ring when $[2\phi/\phi_0]$ is an odd number. With these Majorana fermions, the differential conductance through the lead at the ring (i.e., lead 3 in figure 1) is expected to be different from those without these Majorana fermions. Moreover, since $[2\phi/\phi_0]$ is an odd integer in a large range of ϕ (e.g., $0.25 \leqslant \phi/\phi_0 < 0.75$), these Majorana modes should be robust against the small variation of ϕ.

In this work, we investigate the low energy states and the transport properties of the semiconductor structure addressed above (figure 1). The Rashba spin–orbit coupling and the Zeeman splitting from a magnetic field along either x or z-axis are included. A magnetic flux is applied through the ring which varies the phases of the order parameters in the ring and the two wires (see equation (1)). We find that when the difference of phases in the wires is π, two Majorana modes indeed appear around the ring. However, when the phase difference is zero,
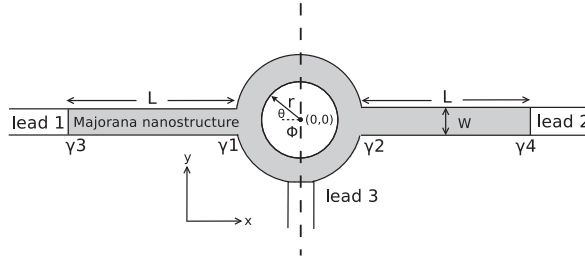
Figure 1. Schematic view of the Majorana nanostructure with two wires connected through a ring. The nanostructure is connected with three normal leads. A magnetic flux Φ is applied through the center of the ring (which is also the origin of the x and z-axes marked as $(0, 0)$ in the figure). Moreover, if the magnetic flux is absent, the nanostructure has the mirror inversion symmetry with the inversion axis shown as the dashed line.

the states around the ring have finite energies. When the ring radius is small, the properties of the differential conductance from leads 1 to 3 in these two cases are different. For the case with the Majorana modes, the interference of the Andreev reflections through these two Majorana modes leads to two differential conductance peaks very close to the zero bias in the bias dependence. For the case without the Majorana modes, the localized states around the ring lead to resonant peaks far away from the zero bias. The different behaviors in the two cases under small ring radius are easily distinguished from each other. Moreover, since the phase difference changes discontinuously from zero to π, the differential conductance peaks also change *discontinuously* from the case without the Majorana modes to those with them. This is a unique property which can be used to identify the existence of the Majorana modes from the other mechanisms leading to the zero-bias peak. Nevertheless, this detection is necessary to be carried out under small ring radius. This is because the energies of the states around the ring under zero phase difference can be close to zero at a large ring radius, which makes the peaks difficult to distinguish from each other. Furthermore, we also find that if the magnetic filed is along the x-axis and the magnetic flux is not applied, the Andreev reflection probability through lead 3 is zero around the zero bias due to the mirror inversion symmetry.

This paper is organized as follows. In section 2, we set up the model and lay out the formalism. In section 3 the results obtained numerically are presented. We summarize and discuss in section 4.

2. Model and formalism

We investigate the semiconductor nanostructure shown in figure 1. The Rashba spin–orbit coupling, proximity-induced superconducting pairing and the Zeeman splitting from a magnetic field are included. Without the leads, the Hamiltonian is expressed as

$$\hat{H}_{\text{eff}} = \hat{H}_{\text{rib}} + \hat{H}_{\text{ring}} + \hat{H}_{\text{SC}} + \hat{H}_{\text{hop}} = \hat{H}_0 + \hat{H}_{\text{hop}}. \tag{2}$$

By discretizing the continuous Hamiltonian over a discrete lattice, the Hamiltonian under the tight-binding approximation is obtained. Here, the width of the wire w is assumed to be very small so that there is only a single 1D mode occupied. Then, for the Hamiltonian of the nanowire, it is treated as one-dimensional one and expressed as [47]

$$\hat{H}_{\text{rib}} = \sum_{\sigma\sigma'\mu} \sum_{i=1}^{L} a_0 \Big[\sigma^n_{\sigma,\,\sigma'} V_n + \big(V_i - \mu_0\big)\delta_{\sigma,\sigma'} \big] c^\dagger_{i\sigma\mu} c_{i\sigma'\mu}$$
$$- \sum_{\langle i,j\rangle\sigma\mu} a_0 t c^\dagger_{i\sigma\mu} c_{j\sigma\mu} + iE_R \sum_{\langle i,j\rangle\sigma\sigma'\mu} a_0 v^x_{ij} \sigma^y_{\sigma\sigma'} c^\dagger_{i\sigma\mu} c_{j\sigma'\mu}. \tag{3}$$

Here, V_n (with $n = x$ or z) stands for the Zeeman splitting from the magnetic field along the **n**-axis; μ_0 represents the chemical potential; $\boldsymbol{\sigma}$ stand for the Pauli matrices; L is the number of sites at each wire; $\mu = -1$ (1) stands for the left(right) wire; $t = \hbar/(2\,m^* a_0^2)$ represents the hopping energy with a_0 denoting the distance between the nearest neighbors in the wire; $V_i = 2t$ stands for the on-site energy; $\langle i, j\rangle$ represents a pair of the nearest neighbors; $v^x_{ij} = \mathbf{e}_x \cdot \mathbf{d}_{ij}$ with $\mathbf{d}_{ij} = (\mathbf{r}_i - \mathbf{r}_j)/|\mathbf{r}_i - \mathbf{r}_j|$; E_R is the Rashba spin–orbit coupling constant. Similarly, the Hamiltonian of the ring reads [46, 48, 49]

$$\hat{H}_{\text{ring}} = \sum_{\sigma\sigma'} \sum_{i=0}^{M-1} \frac{2\pi r}{M} \Big[\sigma^n_{\sigma,\,\sigma'} V_n + \big(V^r_i - \mu_0\big)\delta_{\sigma,\sigma'} \big] c^\dagger_{i\sigma,\,0} c_{i\sigma',0}$$
$$- \sum_{\langle i,j\rangle\sigma} \frac{2\pi r}{M} t_r c^\dagger_{i\sigma,\,0} c_{j\sigma,0} + iE^r_R \sum_{\langle i,j\rangle\sigma\sigma'} \frac{2\pi r}{M} v^\theta_{ij} c^\dagger_{i\sigma,\,0} c_{j\sigma',0}$$
$$\times \Big[\big(\sin\theta_i + \sin\theta_j\big)\sigma^y_{\sigma\sigma'} + \big(\cos\theta_i + \cos\theta_j\big)\sigma^x_{\sigma\sigma'} \Big], \tag{4}$$

in which M is the number of sites in the ring and the distance between the nearest neighbors in the ring is determined by $2\pi r/M$; $c_{i\sigma,0}$ is the annihilation operator for the electron with spin σ at the site i of the ring; $V^r_i = 2t(Ma_0)^2/(2\pi r)^2$; $t_r = t(Ma_0)^2/(2\pi r)^2 e^{i2\pi\phi v^\theta_{ij}/(N\phi_0)}$; $E^r_R = E_R a_0 M e^{i2\pi\phi v^\theta_{ij}/(N\phi_0)}/(4r\pi)$ and $v^\theta_{ij} = \sin[2\pi(j-i)/M]/|\sin[2\pi(j-i)/M]|$. The Hamiltonian for the hopping between the ring and the wires is

$$\hat{H}_{\text{hop}} = -\sum_{\sigma} a_0 t c^\dagger_{L,\,\sigma,\,-1} c_{0\sigma,0} + iE_R \sum_{\sigma\sigma'} a_0 \sigma^y_{\sigma\sigma'} c^\dagger_{L,\,\sigma,\,-1} c_{0\sigma',0}$$
$$- \sum_{\sigma} a_0 t c^\dagger_{\frac{M}{2},\,\sigma,\,0} c_{0\sigma,1} + iE_R \sum_{\sigma\sigma'} a_0 \sigma^y_{\sigma\sigma'} c^\dagger_{\frac{M}{2},\,\sigma,\,0} c_{0\sigma',1} + \text{H.c..} \tag{5}$$

As for the pairing potential, it is given by

$$\hat{H}_{\text{SC}} = \sum_{n\mu} a_0 \Delta_{n,\mu} c^\dagger_{n\uparrow\mu} c^\dagger_{n\downarrow\mu} + \sum_{n=0}^{M-1} \frac{2\pi r}{M} \Delta_{n,0} c^\dagger_{n\uparrow 0} c^\dagger_{n\downarrow 0} + \text{H.c.,} \tag{6}$$

with $\Delta_{n,-1} = |\Delta_0|$, $\Delta_{n,1} = |\Delta_0| \exp(i[2\phi/\phi_0]\pi)$ and $\Delta_{n,0} = |\Delta_0| \exp(i[2\phi/\phi_0]2\pi n/M)$.

Using the convention of the Nambu spinors, $\Psi^\dagger_{i\mu} = (c^\dagger_{i\uparrow\mu}, c^\dagger_{i\downarrow\mu}, c_{i\downarrow\mu}, -c_{i\uparrow\mu})$, this Hamiltonian is rewritten into

$$\hat{H}_{\text{eff}} = \frac{1}{2} \sum_{i\mu j\nu} \Psi^\dagger_{i\mu} H_{\text{BdG}}(i\mu, j\nu) \Psi_{j\nu}, \tag{7}$$

with

$$H_{\text{BdG}}(i\mu, j\nu) = \begin{pmatrix} \hat{H}_0(i\mu, j\nu) & \Delta_{i,\mu}\delta_{ij}\delta_{\mu,\nu} \\ \Delta^*_{i,\mu}\delta_{ij}\delta_{\mu\nu} & -\sigma_y \hat{H}^*_0(i\mu, j\nu)\sigma_y \end{pmatrix} \tag{8}$$

being the Bogoliubov-de Gennes (BdG) Hamiltonian [50]. From this H_{BdG}, the eigenstate $\psi_{i\mu}^n = (u_{i\uparrow\mu}^n, u_{i\downarrow\mu}^n, v_{i\downarrow\mu}^n, v_{i\uparrow\mu}^n)^T$ for the nth state can be obtained numerically under the normalization condition of the wave function $\sum_{i\sigma,\pm 1} a_0 (|u_{i\sigma,\pm 1}^n|^2 + |v_{i\sigma,\pm 1}^n|^2) + \sum_{i\sigma}(2\pi r/M)(|u_{i\sigma,0}^n|^2 + |v_{i\sigma,0}^n|^2) = 1$.

To calculate the transport property of this nanostructure, we connect normal leads to it as shown in figure 1. The Hamiltonian of the lead is given by

$$H_\eta = \sum_{i\sigma\sigma'} a_0 \left[\sigma_{\sigma,\sigma'}^n V_n + \left(V_i - \mu_0 - \mu_\eta \right) \delta_{\sigma,\sigma'} \right] \mathrm{d}_{i\sigma}^{\eta\dagger} \mathrm{d}_{i\sigma'}^\eta$$
$$- \sum_{\langle i,j\rangle\sigma} a_0 t \mathrm{d}_{i\sigma}^{\eta\dagger} \mathrm{d}_{j\sigma}^\eta, \tag{9}$$

in which $\eta = 1, 2, 3$ represent the leads shown in figure 1 and μ_η stands for the difference of the chemical potential between lead η and the nanostructure. The hopping between the leads and the nanostructure is

$$H_{\mathcal{T}} = \sum_{\eta\sigma\sigma'} a_0 \mathcal{T}_{i\sigma,j\sigma'}^\eta \mathrm{d}_{\eta i\sigma}^{\eta\dagger} c_{j\sigma'} + \mathrm{H.c.}, \tag{10}$$

with $\mathcal{T}_{i\sigma,j\sigma'}^\eta = -t\delta_{\sigma\sigma'}$, where i and j stand for the contacting points between the leads and the nanostructure.

We investigate the conductance of the nanostructure at zero temperature. Then, the current through lead η is given by [47]

$$I_\eta = \frac{e}{h} \sum_{\eta'\beta} \int_{\chi_\beta\mu_{\eta'}}^{\mu_\eta} \mathrm{d}\varepsilon \, P_{\eta\eta'}^{e\beta}(\varepsilon), \tag{11}$$

with $\chi_\beta = 1 \, (-1)$ for $\beta = e \, (h)$ and

$$P_{\eta\eta'}^{\alpha\beta}(\varepsilon) = \mathrm{Tr}\left\{ \hat{G}^r(\varepsilon) \hat{\Gamma}_{\eta'}^\beta(\varepsilon) \hat{G}^a(\varepsilon) \hat{\Gamma}_\eta^\alpha(\varepsilon) \right\}. \tag{12}$$

Here, $\hat{G}^{r,a}(\varepsilon)$ are the retarded and advanced Green's functions in the nanostructure connected with the leads; $\hat{\Gamma}_\eta^\alpha(\varepsilon)$ is the self-energy from the electric ($\alpha = e$) or hole part ($\alpha = h$) of the lead η [47].

With the bias applied to the nanostructure, the chemical potentials of the leads are shifted according to $V_{12} = \mu_1 - \mu_2$ and $V_{13} = \mu_1 - \mu_3$. Then, with the further constraint of current conservation

$$\sum_\eta I_\eta = 0, \tag{13}$$

the differential conductance is obtained. In this work, we investigate the differential conductance between two leads without current flowing through the remaining one, i.e., $G_{12} = \frac{\mathrm{d}I_1}{\mathrm{d}V_{12}}|_{I_3=0}$ and $G_{13} = \frac{\mathrm{d}I_1}{\mathrm{d}V_{13}}|_{I_2=0}$. It is noted that when the wires are very long, the transmission between different leads becomes negligible around the zero bias due to the superconducting gap. In this case, only the Andreev reflection contributes and whence equation (11) becomes

$$I_\eta = \frac{e}{h} \int_{-\mu_\eta}^{\mu_\eta} \mathrm{d}\varepsilon \, P_{\eta\eta}^{eh}(\varepsilon). \tag{14}$$

Then, the differential conductance is given by

$$G_{1\eta} = -e\left[P_{\eta\eta}^{eh}\left(\mu_{\eta}\right) + P_{\eta\eta}^{eh}\left(-\mu_{\eta}\right)\right]\partial_{V_{1\eta}}\mu_{\eta}\Big/h. \tag{15}$$

Here, μ_{η} and $\partial_{V_{13}}\mu_{\eta}$ are determined by the current conservation and $V_{1\eta} = \mu_1 - \mu_{\eta}$.

3. Results

We investigate the low energy states and the transport properties of the nanostructure. In our computation, $\Delta_0 = E_R = 0.2t$, $L = 200$, $M = 256$, $\mu_0 = 0.4t$ and $V_n = 0.8t$ unless otherwise specified. It is noted that, with these parameters, the nanostructure is in the topological non-trivial regime, i.e., $\sqrt{\Delta^2 + \mu_0^2} < |V_n| < \sqrt{\Delta^2 + (\mu_0 - 4t)^2}$ [47]. Hence, the Majorana modes are expected to appear at the ends of the nanostructure.

3.1. Majorana states and energy spectrum

In this section, we present the numerical results of the low-energy spectrum and the eigenstates. The radius of the ring is taken to be $r = 2a_0$. Due to the particle-hole symmetry of H_{BdG}, we only investigate the results with positive eigenvalues. The low-energy spectra of the nanostructure under different magnetic fluxes are plotted in figure 2(a) and the magnitudes of the wave functions for the lowest two states are shown in figures 2(b) and (c). It is noted that the energy spectra with the Zeeman splitting from a magnetic field along either x- or z-axis are similar. Hence, we only plot the results with a magnetic field in z-axis in figure 2.

From figure 2(a), one finds that for the case with the magnetic flux $\phi = 0$ (red dots), the eigenvalue ε_1 is extremely small while the other eigenvalues are much higher. Moreover, from the distribution of the wave functions shown in figure 2(b), it is found that the lowest state mainly distributes at the ends of the nanostructure and the second lowest state mainly distributes around the ring. These behaviors can be easily understood as follows. If the ring is removed from the nanostructure, it is well known that Majorana modes exist at the ends of the left and right wires (marked as γ_1 to γ_4 in figure 1). With a ring connecting these two wires, the Majorana modes close to the ring in each wire (i.e., γ_1 and γ_2 in figure 1) interact with each other and form the second lowest state. For the remaining Majorana modes (γ_3 and γ_4 in figure 1), they compose the lowest eigenstate with the corresponding non-zero eigenvalue coming from the interactions between them. To further confirm this, we also calculate the case with a shorter wire length $L = 100$ (blue squares). It is shown that ε_1 increases markedly while ε_2 remains almost unchanged, which is consistent with the feature of the interacting Majorana fermions.

We further investigate the influence of the magnetic flux by increasing ϕ. The results are similar to the case with $\phi = 0$ until $\phi = 0.25\phi_0$ where $[2\phi/\phi_0] = 1$ and $\Delta_{n,-1} = -\Delta_{n,1}$. The low energy spectrum is plotted as yellow triangles in figure 2(a). It is shown that both the lowest and the second lowest energies are very close to zero. Furthermore, from the magnitudes of the wave functions for the lowest two eigenstates shown in figure 2(c), it is found that the two wave functions distribute both around the ring and at the ends of the nanostructure. These behaviors indicate the existence of the Majorana modes around the ring. These Majorana modes interact with those at the ends of the nanostructure (γ_3 and γ_4) which leads to the small non-zero eigenvalues (i.e., ε_1 and ε_2). Since the interaction between them decreases exponentially with the increase of their distance, we also calculate the case with $L = 300$, which leads to much
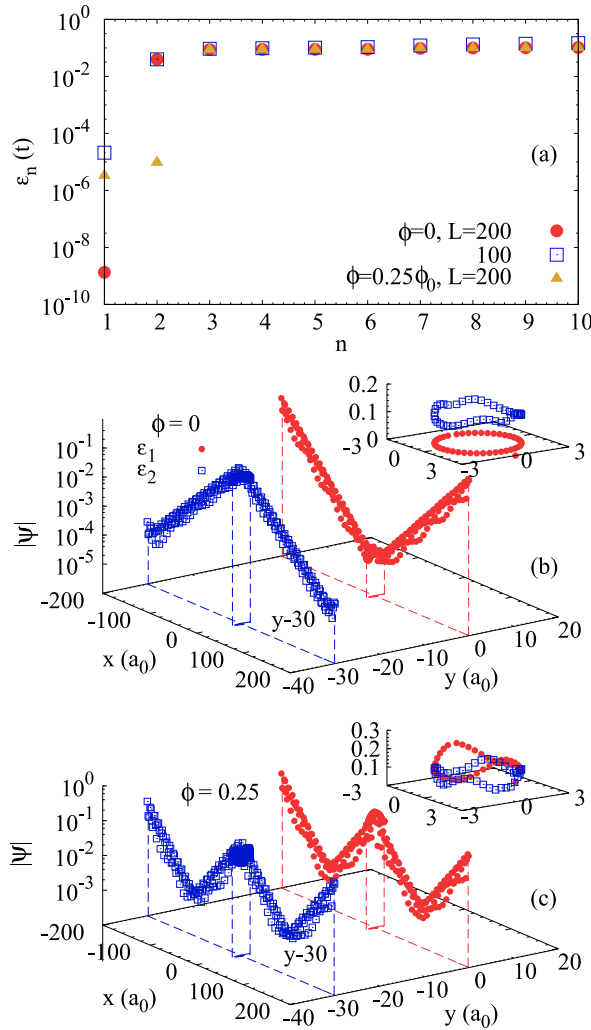
Figure 2. (a) Low energy spectra with different wire lengths for $\phi = 0$ and $0.25\phi_0$, respectively. n labels the eigenvalues of H_{BdG} starting with zero energy. (b) and (c) Magnitudes of the wave functions of the lowest two states (ϵ_1 and ϵ_2) for $\phi = 0$ and $0.25\phi_0$, respectively. Those of the second lowest states (blue squares) are shifted by $30a_0$ along the z-axis for clarity. The insets zoom the wave functions at the ring of the nanostructure. The magnetic field is along the **z**-axis and the radius of the ring is $2a_0$.

lower ϵ_1 (2.5×10^{-8t}) and ϵ_2 (7.7×10^{-8t}). This behavior confirms the existence of the Majorana fermions around the ring. It is noted that this result is similar to those appearing in two connected nanostructures with a π phase difference of the order parameters investigated in the literature [41–44].

3.2. Electric conductance

In this section, we investigate the influence of the Majorana modes on the conductance by varying the magnetic flux ϕ. Here, the wires are long enough and only the Andreev reflection contributes to the transport. Thus, the differential conductance through each lead is mainly determined by the states around the lead which helps to show their influence clearer. It is noted

that the property of the differential conductance between leads 1 and 2, i.e., G_{12}, is mainly determined by the Majorana modes at the ends of the nanostructure (γ_3 and γ_4 shown in figure 1), which is similar to previous works in the literature [47, 51]. Hence, it is not shown in the figure. In this work we only concentrate on the differential conductance between leads 1 and 3, i.e., G_{13}.

We first focus on the case with a short ring radius (i.e., $r = 2a_0$). For the case with $\phi = 0.25\phi_0$ where the phase difference of the order parameters in the two wires is π (i.e., with the Majorana modes around the ring), two conductance peaks appear in the bias voltage V_{13} dependence which are very close to the zero bias (i.e., $V_{13} = 0$) and hence lead to a sharp valley between them as shown in figure 3(a). With the increase of ϕ to $0.4\phi_0$, where the phase difference is still π, the valley is shown to become milder. Nevertheless, the corresponding peaks are still close to the zero bias. On contrast, for the case with zero phase difference (i.e., without any Majorana modes around the ring), e.g., $\phi = 0$ and $0.1\phi_0$, the peaks appearing in the bias dependence become close to the energies of the second lowest states (marked as arrows) which are far away from zero. This behavior is quite different from that with the Majorana modes and hence can be used to distinguish the two cases. Moreover, since the phase difference varies discontinuously from zero to π, the conductance peaks without the Majorana modes also change to the ones with them *discontinuously*. This is a unique property of the Majorana modes which helps to exclude the other mechanisms leading to the zero-bias peaks.

Here, we give an analytical investigation on the properties of the differential conductance peaks in the cases with and without the Majorana modes around the ring. The differential conductance G_{13} is determined by the Andreev reflections through leads 1 and 3 under the constraint of current conservation (which determines μ_1 and μ_3 incorporating with $V_{13} = \mu_1 - \mu_3$). For the Andreev reflection through lead 1, it is strong due to the Majorana mode near lead 1 (i.e., γ_3) and the corresponding P_{11}^{eh} is almost 1 in our parameter range. In contrast, the Andreev reflection through lead 3 varies largely and the corresponding P_{33}^{eh} is found to be zero around the zero bias. Therefore, due to the current conservation (equations (13) and (14)) and $V_{13} = \mu_1 - \mu_3$, μ_3 is close to $-V_{13}(\partial_{V_{1\eta}}\mu_\eta$ is close to -1) and the differential conductance is mainly determined by the Andreev reflection through lead 3 (i.e., $P_{\eta\eta}^{eh}(\mu_3) + P_{\eta\eta}^{eh}(-\mu_3)$, see equation (15)). With this understanding, the conductance peaks close to the zero bias in the case with π phase difference are understood to come from the Andreev reflection through the Majorana modes around the ring. And the peaks close to the energies of the second lowest states in the case with zero phase difference are understood to come from the resonance Andreev reflection through these subgap states (which are also localized around the ring, see figure 2(b)). It is noted that both the contributions of the Majorana modes (with π phase difference) and the second lowest states (with zero phase difference) can be studied formally by investigating the Andreev reflection through states ψ^n and ψ^{-n} with $\psi^{-n} = \psi^{n\dagger}$ due to the partial-hole symmetry. Here, by setting ψ^n being the fermion mode composed by the Majorana modes γ_{r1} and γ_{r2} around the ring (i.e., $\psi^n = (\gamma_{r1} + i\gamma_{r2})/\sqrt{2}$) and setting the corresponding energies $\varepsilon_n = \varepsilon_{-n} = 0$, the result describes the tunneling through the two Majorana modes. Meanwhile, by setting ψ^n being the second lowest state (i.e., $n = 2$) and using $\varepsilon_2 = -\varepsilon_{-2} \neq 0$, it describes the tunneling through the second lowest states.

Since the lead 3 is connected to the nanostructure at one point, the couplings between these two states ψ^n and ψ^{-n} to the lead 3 are determined by their wave functions at the connecting point which are described by $\psi^n = (u_\uparrow, u_\downarrow, v_\downarrow, v_\uparrow)^T$ and $\psi^{-n} = \psi^{n\dagger}$ in the Nambu spinors. Then the approximate formula is given as (see the appendix)
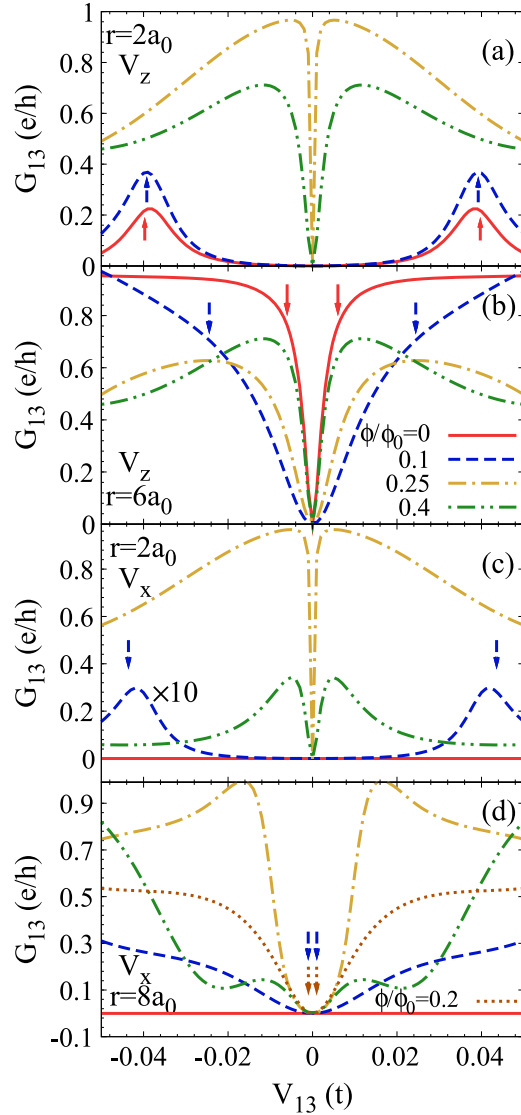
Figure 3. Differential conductance for cases with the magnetic field along the z-axis with (a) $r = 2a_0$ and (b) $r = 6a_0$ as well as the case along the x-axis with (c) $r = 2a_0$ and (d) $r = 8a_0$ under different magnetic fluxes. The results with $\phi = 0.1\phi_0$ (blue dashed curve) in (c) is enlarged by 10 for clarity. The arrows indicate the energies of the corresponding second lowest states of the nanostructure.

$$P^{eh}(\varepsilon) = 64|u_\downarrow|^2|v_\downarrow|^2\Gamma_L^e\Gamma_L^h\varepsilon^2\big/D(\varepsilon). \tag{16}$$

Here, $D(\varepsilon) = [4(\varepsilon_n^2 - \varepsilon^2) + \Gamma_L^e\Gamma_L^h(|u_\downarrow|^2 - |v_\downarrow|^2)^2]^2 + 4[(\Gamma_L^e + \Gamma_L^h)\varepsilon(|u_\downarrow|^2 + |v_\downarrow|^2) + (\Gamma_L^e - \Gamma_L^h)\varepsilon_n (|u_\downarrow|^2 - |v_\downarrow|^2)]^2$. From this equation, $P^{eh}(0)$ is found to be zero which explains the valley in our results. Moreover, under the approximation $\Gamma_L^e = \Gamma_L^h$ (valid around the zero bias), one further finds that the peaks locate at $\pm\sqrt{\varepsilon_n^2 + (|u_\uparrow|^2 - |v_\uparrow|^2)^2\Gamma_L^e\Gamma_L^h/4}$. From this result, one understands that both $|u_\uparrow|^2 - |v_\uparrow|^2$ and the energy of the state ε_n influence the location of the corresponding peaks (as well as the steepness of the valley between them). Nevertheless, if the energy ε_n of the
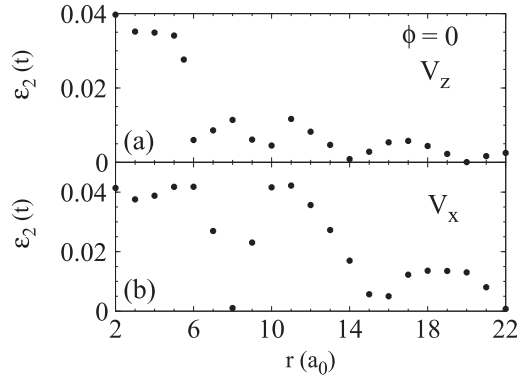
Figure 4. The ring radius dependence of the energy of the second lowest state ε_2 with the Zeeman splitting from the magnetic field along the (a) z- and (b) x-axes. Here, the magnetic flux $\phi = 0$.

second lowest state in the case with zero phase difference (e.g., $\phi = 0$ and $0.1\phi_0$) is much larger than $\sqrt{(|u_\uparrow|^2 - |v_\uparrow|^2)^2 \Gamma_L^e \Gamma_L^h / 4}$, the corresponding peaks will be far away from those due to the Majorana modes (i.e., $\varepsilon_n = 0$ in the case with π phase difference, e.g., $\phi = 0.25\phi_0$ and $0.4\phi_0$) as shown in figure 3(a).

  With this understanding, we further investigate the case with a different ring radius. The variation of the ring radius changes the couplings between the states in different wires. As a result, the energies of the second lowest states in the case with zero phase difference can be close to zero, making the location of the peaks (or the steepness of the corresponding valley) difficult to be distinguished from those due to the Majorana modes. This can be seen in figure 3(b) in which the differential conductance G_{13} is plotted against the bias voltage V_{13} with $r = 6a_0$. For the case with zero phase difference (i.e., without any Majorana modes), it is shown that the second lowest eigenvalues (marked by the arrows) can be very close to zero (e.g., $\phi = 0$). Then, the steepness of the valley is mainly determined by $|u_\uparrow|^2 - |v_\uparrow|^2$ as the case due to the Majorana modes. As a result, the conductance valleys with (e.g., $\phi = 0.4\phi_0$) and without (e.g., $\phi = 0$)[1] the Majorana modes can be similar. This makes the two cases difficult to be distinguished from each other. These results suggest the importance to rule out the second lowest states in the case with zero phase difference. Thus, we further show the energies of the second lowest states at $\phi = 0$ as the function of the ring radius in figure 4(a). It is shown that, with the increase of the ring radius, the energy of the second lowest state oscillates and tends to decrease. Nevertheless, the energies in the cases with $r < 5a_0$ are always large. This indicates that, to identify the existence of the Majorana modes around the ring, it is necessary to detect in the case with small ring radius ($<5a_0$).

  In addition to the case with a magnetic field along the z-axis, we further investigate the case with the magnetic field along the x-axis as shown in figures 3(c) and (d). Since the properties of the energy spectra for these two magnetic field directions are similar (see figure 4), the corresponding conductances are also expected to be similar as confirmed by the cases with

---

[1] The differential conductances for the cases with $\phi = 0$ and $0.1\phi_0$ shown in figure 3(b) do not exhibit peak structure in the investigated energy range. This comes from the contribution of the third lowest state, whose energy is also small when the ring radius is large ($\varepsilon_3 = 0.046t$ for $\phi = 0$ and $0.044t$ for $\phi = 0.1\phi_0$ in this case).

the magnetic fluxes under both small ($r = 2a_0$ shown in figure 3(c)) and large ($r = 8a_0$ shown in figure 3(d)) ring radii. Nevertheless, if the magnetic flux is not applied (i.e., $\phi = 0$), it is shown in figures 3(c) and (d) that the corresponding differential conductances keep zero in our parameter range. This special property comes from the mirror inversion symmetry of the nanostructure which is understood as follows.

With the magnetic field along the x-axis applied to the nanostructure, the spin degeneracy in the lead is split into σ_x^+ and σ_x^-. Since the Zeeman splitting is larger than the chemical potential, only the lower eigenstate σ_x^- in the lead contributes to the conductance. This eigenstate only couples the state in the nanostructure with spin parallel to it, whose component in the corresponding wave function ψ^n is $(u_\uparrow - u_\downarrow)/\sqrt{2}$ for the electron part and $(v_\uparrow + v_\downarrow)/\sqrt{2}$ for the hole part. Then, the Andreev reflection probability is understood to be proportional to $(u_\uparrow - u_\downarrow)(v_\uparrow + v_\downarrow)$ (see also the appendix). For our nanostructure without the magnetic flux, the Hamiltonian is invariant under the mirror inversion with the inversion axis along the lead 3 (the corresponding operator is $\boldsymbol{\pi}\sigma_x$, with $\boldsymbol{\pi}^\dagger \mathbf{x} \boldsymbol{\pi} = -\mathbf{x}$). Then, at the point contacting with lead 3, each non-degenerate eigenstate of the nanostructure has to satisfy the relation $\psi^n = \pm \sigma_x \psi^n$, i.e., $(u_\uparrow, u_\downarrow, v_\downarrow, v_\uparrow)^T = \pm(u_\downarrow, u_\uparrow, v_\uparrow, v_\downarrow)^T$. As a result, $u_\uparrow - u_\downarrow = 0$ or $v_\uparrow + v_\downarrow = 0$. Hence the Andreev reflection through lead 3 is forbidden, leading to the zero G_{13}. It is noted that this analysis is valid only when several states contribute to the conductance. If the bias is large and the continuum states are involved, G_{13} becomes non-zero.

4. Summary and discussion

In summary, we have investigated the Majorana fermions in a semiconductor nanostructure with two long wires connected through a ring. The nanostructure is in the proximity of a superconductor and the Rashba spin–orbit coupling, proximity-induced superconducting pairing and the Zeeman splitting from a magnetic field are included. A magnetic flux is applied through the center of the ring. Then, due to the fluxoid quantization and the thermodynamic equilibrium of the supercurrent in the superconducting ring [46], the phase difference between the order parameters of the two semiconductor wires is zero or π. We show that when it is zero, the states in the two wires are coupled through the ring and the eigenstates localized around the ring have finite energies (i.e., there is no Majorana modes around the ring). Nevertheless, when the phase difference becomes π, two Majorana states appear around the ring without interacting with each other.

We further investigate the transport property of the nanostructure by connecting two normal leads to the wires and a third one directly to the ring. The low bias differential conductance between one of the leads connected at the wire and the one at the ring is mainly limited by the small Andreev reflection probability through the lead connected at the ring, due to the current conservation. Hence, in both cases, i.e., with and without the Majorana modes around the ring, this differential conductance can show very distinct features. In the case with the Majorana modes (i.e., with π phase difference), the bias dependence of the differential conductance exhibits two peaks very close to the zero bias due to the interference of the Andreev reflections through these two Majorana modes. On contrast, in the case without the Majorana modes (i.e., with zero phase difference), it shows peaks far away from the zero bias if the ring radius is small. This is due to the resonant Andreev reflections through the localized states with finite energies. The behaviors in these two cases under small ring radius can be

easily distinguished from each other. This is a unique property of the Majorana modes which helps to exclude the other mechanisms leading to the zero-bias peak. Nevertheless, we also point out that if the ring radius becomes large, the energies of the states in the case with the zero phase difference can be very close to zero, which makes the corresponding peaks difficult to be distinguished from those due to the Majorana modes in the case with π phase difference. Hence, to identify the Majorana modes, small ring radius is a must.

In addition, we also find that due to the mirror symmetry of the nanostructure, the Andreev reflection through the lead connected at the ring (which is along the inversion axis) is forbidden around the zero bias if the magnetic field is parallel to the wires and the magnetic flux is absent.

Finally we address the feasibility of our model. If the nanostructure is realized in InAs, our parameters correspond to $\Delta_0 = 0.53$ meV and $t = 2.64$ meV [52]. Then, to make sure that only the lowest subband is occupied as we assume in the model, the width of the wire w needs to be less than 32 nm (the corresponding second subband energy $\hbar^2 4\pi^2/(2\,m^*w^2)$ is larger than $10t$). As for the temperature T, it limits the resolution of the conductance measurement. If $k_B T$ is larger than the bias difference between the differential conductance peaks, these peaks can not be distinguished from each other. From figures 3(a) and (c), the bias difference between the differential conductance peaks for the case without Majorana modes around the ring (the phase difference $\phi < 0.25\phi_0$) is larger than $\Delta V = 0.08t = 0.21$ meV. This corresponds to about 2.6 K, which is experimental available [25, 26]. Therefore, these two peaks can be distinguished from each other and hence can be distinguished from those due to the Majorana modes around the ring (the corresponding $\Delta V < 0.02t$ as shown in figures 3(a) and (c)). We further discuss the influence of the electron–electron Coulomb interaction beyond the mean field level (i.e., beyond just using the superconducting gap Δ_0). Although the Coulomb interaction degrades the superconducting gap [53], it also greatly expands the parameter range for the appearance of the Majorana modes [54]. Therefore, the qualitative behaviors of the differential conductance predicted in this work are still valid as long as the Majorana modes exist.

Acknowledgments

Appendix. Interference effect of the tunneling through two Majorana modes

In this section, we present the interference effect of the Andreev reflections through two states ψ^n and ψ^{-n}. Due to the partial-hole symmetry, $\psi^{n\dagger} = \psi^{-n}$ and their corresponding energies satisfy $\varepsilon_n = -\varepsilon_{-n}$. Then, the Green function is written as

$$\hat{G}^r(\varepsilon) = \left[\varepsilon - \begin{pmatrix} \varepsilon_n & 0 \\ 0 & -\varepsilon_n \end{pmatrix} + \frac{i}{2}\left(\Gamma_e + \Gamma_h\right)\right]^{-1}, \tag{A.1}$$

in which $-i\Gamma_e/2$ stands for the self-energy from the electron part of the lead and $-i\Gamma_h/2$ from the hole part. They are expressed as

$$-\frac{i}{2}\Gamma_{e/h}(\varepsilon) = \mathcal{T}G_L^{e/h}\mathcal{T}^\dagger, \tag{A.2}$$

with G_L^e and G_L^h standing for the electron and hole Green functions in the lead and $\mathcal{T}$ representing the hopping matrix from the two states to the lead.

For the case with the magnetic field along the z-axis, considering that the Majorana modes appear only when the Zeeman splitting is larger than $\sqrt{\mu_0^2 + |\Delta_0|^2}$, the Green functions in the lead can be expressed as

$$G_L^e = \begin{pmatrix} 0 & 0 & 0 & 0 \\ 0 & -\dfrac{i}{2}\Gamma_L^e & 0 & 0 \\ 0 & 0 & 0 & 0 \\ 0 & 0 & 0 & 0 \end{pmatrix}, \text{ and } G_L^h = \begin{pmatrix} 0 & 0 & 0 & 0 \\ 0 & 0 & 0 & 0 \\ 0 & 0 & -\dfrac{i}{2}\Gamma_L^h & 0 \\ 0 & 0 & 0 & 0 \end{pmatrix}$$

in the Nambu spinor basis. On the other hand, for the case with the magnetic field along the x-axis, they are expressed as

$$G_L^e = -\frac{i}{4}\begin{pmatrix} \Gamma_L^e & -\Gamma_L^e & 0 & 0 \\ -\Gamma_L^e & \Gamma_L^e & 0 & 0 \\ 0 & 0 & 0 & 0 \\ 0 & 0 & 0 & 0 \end{pmatrix},$$

$$\text{and } G_L^h = -\frac{i}{4}\begin{pmatrix} 0 & 0 & 0 & 0 \\ 0 & 0 & 0 & 0 \\ 0 & 0 & \Gamma_L^h & \Gamma_L^h \\ 0 & 0 & \Gamma_L^h & \Gamma_L^h \end{pmatrix}.$$

As for the hopping matrix, it is expressed as

$$\mathcal{T} = \begin{pmatrix} u_\uparrow^* & u_\downarrow^* & v_\downarrow^* & v_\uparrow^* \\ -v_\uparrow & v_\downarrow & u_\downarrow & -u_\uparrow \end{pmatrix}, \tag{A.3}$$

with $(u_\uparrow, u_\downarrow, v_\downarrow, v_\uparrow)^T$ being the Nambu spinors of ψ^n at the point of the nanostructure connecting with lead 3. Then, substituting equations (A.1) and (A.2) into equation (12), the transmission coefficient for the case with the magnetic field along the z-axis is given by equation (16) and that along the x-axis is

$$P^{eh} = \Gamma_L^e\Gamma_L^h \left| 16(u_\downarrow - u_\uparrow)(v_\downarrow^* + v_\uparrow^*)\varepsilon/D(\varepsilon) \right|^2, \tag{A.4}$$

with $D(\varepsilon) = |u_\downarrow - u_\uparrow|^4\Gamma_L^e\Gamma_L^h - 2|u_\downarrow - u_\uparrow|^2\{\Gamma_L^e\Gamma_L^h|v_\downarrow + v_\uparrow|^2 + 2i[\Gamma_L^h(\varepsilon - \varepsilon_n) + \Gamma_L^e(\varepsilon + \varepsilon_n)]\} - [4(\varepsilon + \varepsilon_n) + i\Gamma_L^e|v_\downarrow + v_\uparrow|^2][4(\varepsilon - \varepsilon_n) + i\Gamma_L^h|v_\downarrow + v_\uparrow|^2]$.

References

[1] Read N and Green D 2000 *Phys. Rev.* B **61** 10267
[2] Ivanov D A 2001 *Phys. Rev. Lett.* **86** 268
[3] Kitaev A Y 2003 *Ann. Phys.* **303** 2
[4] Nayak C, Simon S H, Stern A, Freedman M and das Sarma S 2008 *Rev. Mod. Phys.* **80** 1083

[5] Alicea J, Oreg Y, Refael G, von Oppen F and Fisher M P A 2011 *Nat. Phys.* **7** 412

[6] Sau J D, Clarke D J and Tewari S 2011 *Phys. Rev.* B **84** 094505

[7] Halperin B I, Oreg Y, Stern A, Refael G, Alicea J and von Oppen F 2012 *Phys. Rev.* B **85** 144501

[8] Fu L and Kane C L 2008 *Phys. Rev. Lett.* **100** 096407

[9] Tanaka Y, Yokoyama T and Nagaosa N 2009 *Phys. Rev. Lett.* **103** 107002

[10] Linder J, Tanaka Y, Yokoyama T, Sudbø A and Nagaosa N 2010 *Phys. Rev. Lett.* **104** 067001

[11] Oreg Y, Refael G and von Oppen F 2010 *Phys. Rev. Lett.* **105** 177002

[12] Benjamin C and Pachos J K 2010 *Phys. Rev.* B **81** 085101

[13] Sau J D, Tewari S, Lutchyn R M, Stanescu T D and das Sarma S 2010 *Phys. Rev.* B **82** 214509

[14] Nakosai S, Tanaka Y and Nagaosa N 2012 *Phys. Rev. Lett.* **108** 147003

[15] Tanaka Y, Sato M and Nagaosa N 2012 *J. Phys. Soc. Japan* **81** 011013

[16] Ghaemi P and Wilczek F 2012 *Phys. Scr.* **T146** 014019

[17] Nakosai S, Budich J C, Tanaka Y, Trauzettel B and Nagaosa N 2013 *Phys. Rev. Lett.* **110** 117002

[18] Nadj-Perge S, Drozdov I K, Bernevig B A and Yazdani A 2013 *Phys. Rev.* B **88** 020407(R)

[19] Klinovaja J, Stano P, Yazdani A and Loss D 2013 *Phys. Rev. Lett.* **111** 186805

[20] Sau J D and Tewari S 2013 *Phys. Rev.* B **88** 054503

[21] Stanescu T D and Tewari S 2013 *J. Phys.: Condens. Matter* **25** 233201

[22] Rokhinson L P, Liu X and Furdyna J K 2012 *Nat. Phys.* **8** 795

[23] Williams J R, Bestwick A J, Gallagher P, Hong S S, Cui Y, Bleich A S, Analytis J G, Fisher I R and Goldhaber-Gordon D 2012 *Phys. Rev. Lett.* **109** 056803

[24] Sasaki S, Kriener M, Segawa K, Yada K, Tanaka Y, Sato M and Ando Y 2011 *Phys. Rev. Lett.* **107** 217001

[25] Das A, Ronen Y, Most Y, Oreg Y, Heiblum M and Shtrikman H 2012 *Nat. Phys.* **8** 887

[26] Mourik V, Zuo K, Frolov S M, Plissard S R, Bakkers E P A M and Kouwenhoven L P 2012 *Science* **336** 1003

[27] Deng M T, Yu C L, Huang G Y, Larsson M, Caroff P and Xu H Q 2012 *Nano Lett.* **12** 6414

[28] Churchill H O H, Fatemi V, Grove-Rasmussen K, Deng M T, Caroff P, Xu H Q and Marcus C M 2013 *Phys. Rev.* B **87** 241401(R)

[29] Lee E J H, Jiang X, Houzet M, Aguado R, Lieber C M and Franceschi S De 2014 *Nat. Nanotechnology* **9** 79

[30] Yamakage A, Yada K, Sato M and Tanaka Y 2012 *Phys. Rev.* B **85** 180509(R)

[31] Bolech C J and Demler E 2007 *Phys. Rev. Lett.* **98** 237002

[32] Law K T, Lee P A and Ng T K 2009 *Phys. Rev. Lett.* **103** 237001

[33] Flensberg K 2010 *Phys. Rev.* B **82** 180516(R)

[34] Prada E, San-Jose P and Aguado R 2012 *Phys. Rev.* B **86** 180503(R)

[35] Lin C-H, Sau J D and das Sarma S 2012 *Phys. Rev.* B **86** 224511

[36] Diez M, Dahlhaus J P, Wimmer M and Beenakker C W J 2012 *Phys. Rev.* B **86** 094501

[37] Liu J, Potter A C, Law K T and Lee P A 2012 *Phys. Rev. Lett.* **109** 267002

[38] Kells G, Meidan D and Brouwer P W 2012 *Phys. Rev.* B **86** 100503(R)

[39] Chang W, Manucharyan V E, Jespersen T S, Nygard J and Marcus C M 2013 *Phys. Rev. Lett.* **110** 217005

[40] Rainis D, Trifunovic L, Klinovaja J and Loss D 2013 *Phys. Rev.* B **87** 024515

[41] Fu L and Kane C L 2009 *Phys. Rev.* B **79** 161408(R)

[42] Lutchyn R M, Sau J D and das Sarma S 2010 *Phys. Rev. Lett.* **105** 077001

[43] Kwon H-J, Sengupta K and Yakovenko V M 2004 *Eur. Phys. J.* B **37** 349

[44] Xu Y, Mao L, Wu B and Zhang C 2014 arXiv:1401.3777

[45] das Sarma S, Sau J D and Stanescu T D 2012 *Phys. Rev.* B **86** 220506(R)

[46] Pientka F, Romito A, Duckheim M, Oreg Y and von Oppen F 2013 *New J. Phys.* **15** 025001

[47] Zhou Y and Wu M W 2014 *J. Phys.: Condens. Matter* **26** 065801

[48] Meijer F E, Morpurgo A F and Klapwijk T M 2002 *Phys. Rev.* B **66** 033107

[49] Joibari F K, Blanter Ya M and Bauer G E W 2013 *Phys. Rev.* B **88** 115410

[50] de Gennes P G 1966 *Superconductivity of Metals and Alloys* (New York: Benjamin)

[51] Lim J S, López R and Serra L 2012 *New J. Phys.* **14** 083020
[52] Stanescu T D, Lutchyn R M and das Sarma S 2011 *Phys. Rev.* B **84** 144522
[53] Gangadharaiah S, Braunecker B, Simon P and Loss D 2011 *Phys. Rev. Lett.* **107** 036801
[54] Stoudenmire E M, Alicea J, Starykh O A and Fisher M P A 2011 *Phys. Rev.* B **84** 014503